# Nonhematotoxic Naphthalene Diimide Modified by Polyamine: Synthesis and Biological Evaluation

Yuxia Wang,[†] Xingbo Zhang,[‡] Jin Zhao,[§] Songqiang Xie,*,[†] and Chaojie Wang*,[§]

[†]Institute of Chemical Biology, [‡]Department of Chemistry, and [§]Key Lab of Natural Medicine and Immune Engineering, Henan University, Henan, China

ABSTRACT: With the aim of up-regulating antitumor efficacy and down-regulating adverse effects, three types of aromatic imide and diimides were designed to couple with different polyamines. The in vitro assays revealed that two naphthalene diimide–polyamine conjugates could inhibit the growth of multiple cancer cell lines more potently than amonafide. **9f**, the most potent compound, was verified to efficiently induce apoptosis via a ROS mediated mitochondrial pathway in a preliminary mechanistic study. The comprehensive in vivo trials on three H22 tumor transplant models demonstrated that **9f** improved the indexes in terms of inhibitive effect and lifespan extension and reduced the hematotoxicity which is one of main drawbacks of amonafide. More importantly, the obviously elevated ability in preventing lung cancer metastasis was observed, which increased the value of **9f** as a promising lead compound. This work supported that the versatile function of polyamines may endow some intriguing biological features to the parent drugs.
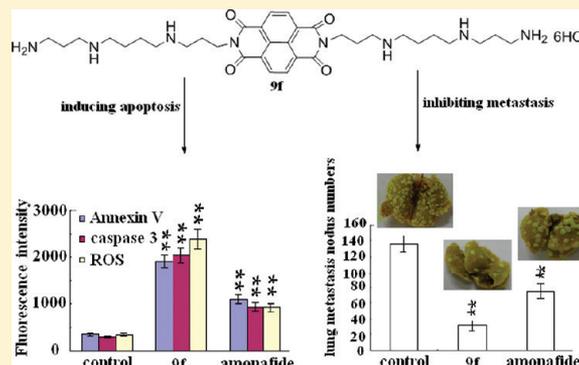
1. INTRODUCTION

Cancer is well-known as one of the most fatal diseases featured by eternal cell proliferation and the spreading of cancerous cells to other tissues by invasion or metastasis. Undoubtedly, cancer is an unsolved problem to date, and the rapid growth in cancer cases represents a real crisis for public health in the world. In spite of side effects caused by chemotherapy treatment such as the occurrence of myelosuppression and the development of drug resistance, it is still recognized as the main choice to prolong the patient's life. Therefore, the discovery of novel, selective, efficient, and safe drugs for cancer chemotherapy remains an urgency and high priority for medicinal research.

In therapeutics, aromatic imides have been recognized as a promising group of antitumor agents. Some phathalimides such as thalidomide and lenalidomide are now in clinical use.[1,2] Naphthalimides are also a class of intriguing pharmacophores because of their broad bioactivities.[3,4] Many naphthalimides reached clinical trials, but most of them were abandoned because of various adverse effects such as dose-limiting bone marrow toxicity. As a representative, amonafide (Figure 1) is currently undergoing phase III clinical trials in combination with cytarabine in patients with acute myeloid leukemia.[5] In view of both the evidenced antitumor activity and negative effects of these compounds, extensive efforts including the modification of side chain, aromatic ring system, and the substituents on the ring have been attempted to search for more selective naphthalimides to improve the potency and reduce the adverse effects (Figure 1).[6,7] In an excellent paper with comprehensive in vivo messages, Kiss et al. reported the amonafide derivatives by the modification of amino group on

the aromatic ring to prevent hematotoxic results.[8] Qian et al. suggested a strategy to furnish multitargeted naphthalimides by varying the side chains and substituents with polyamine moieties and lipophilic alkyl chains.[9] Naphthalene diimides such as N-BDMPrNDI (Figure 1) are attractive DNA intercalators similar to naphthalimides.[10] A recent report of Tumiatti et al. focused on the naphthalene diimides, which are found to be more active than their corresponding mono-imides.[11]

Diverse polyamine derivatives have been extensively studied for their intriguing bioactivities.[12−15] In recent years, polyamine conjugates have attracted increasing attention because the antitumor agents modified by polyamines may possess improved bioactivity and cell selectivity.[16−18] After efforts of several decades, F14512, an epipodophyllotoxin–spermine conjugate, is perhaps the most promising compound which is presently being evaluated in phase I trials.[19,20] There are several reports about naphthalimide polyamine conjugates as well.[21,22] Our work demonstrated that the naphthalimide coupled with spermidine or homospermidine (Figure 1, MNISpd, MNIHspd) exhibited antineoplastic potency and, more importantly, excellent cell selectivity in a normal versus transformed cells screen.[23−25] These findings stimulated us to search for more promising imide scaffolds suitable to polyamine modification. We report herein three kinds of aromatic imide/diimides (with anhydrides as starting materials), which are coupled with diverse polyamine motifs (Figure 2). In addition
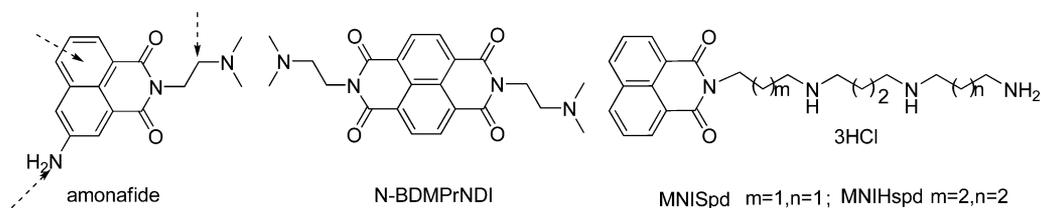
Figure 1. Chemical structures of amonafide, N-BDMPrNDI, MNISpd, and MNIHspd.

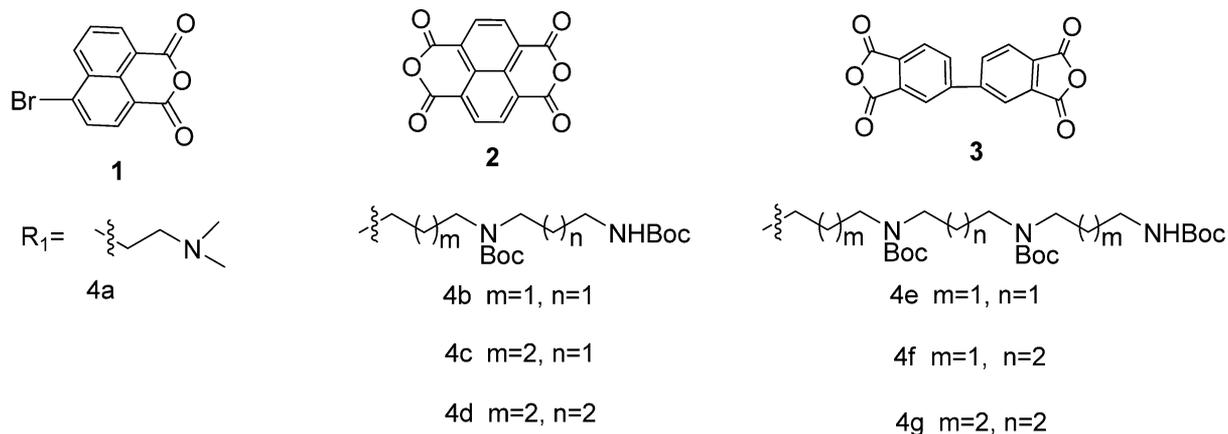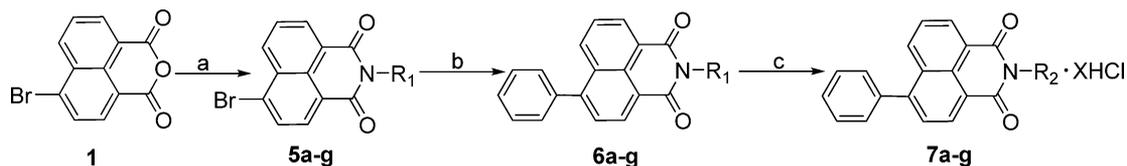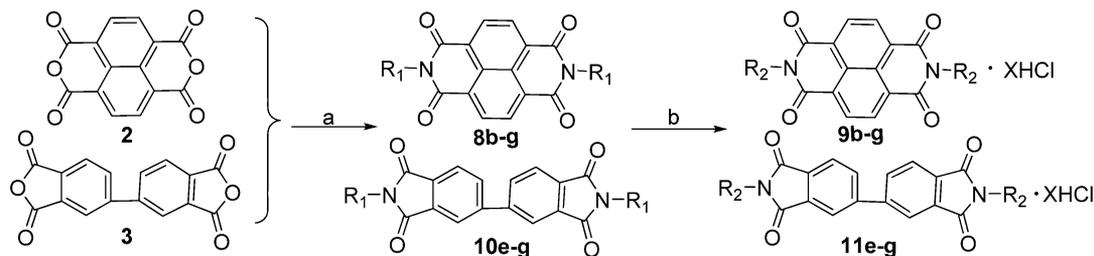**Figure 2.** Building blocks of the designed library.

Scheme 1[a]

[a](a) 1.0 equiv of R_1NH_2, EtOH, reflux, 3 h; (b) 1.0 equiv of $PhB(OH)_2$, 1.5 equiv of K_2CO_3, catalytic amount of TBAB and $PdCl_2$, toluene, reflux; (d) EtOH, 4 M HCl, room temperature, overnight.

Scheme 2[a]

[a](a) 1.0 equiv of R_1NH_2, EtOH/toluene, reflux; (b) EtOH, 4 M HCl, room temperature, overnight.

to the routine in vitro evaluation, in vivo experiments are designed to provide more data for future drug development.
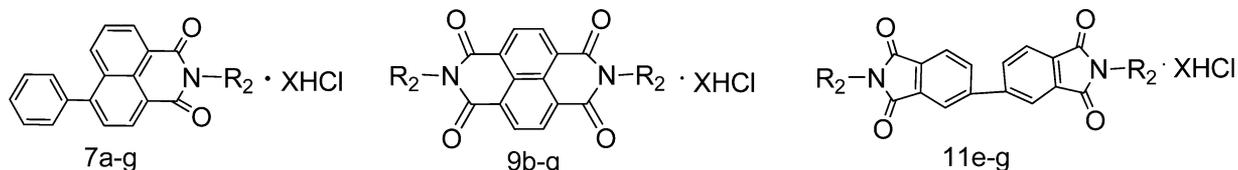
2. RESULTS AND DISCUSSION

2.1. Chemistry. The phenyl substituted naphthalimide–polyamine compounds (**7a–g**) were synthesized according to Scheme 1. Intermediates **5a–g** were obtained by the condensation of R_1NH_2 (**4**; the Boc protected polyamines were prepared by a modified procedure reported previously[23,24]) with 4-bromo-1,8-naphthalic anhydride (**1**). The Suzuki coupling reaction of **5** with phenylboronic acid catalyzed by $PdCl_2$ gave intermediates **6**,[26,27] and their Boc groups in the polyamine skeleton were subsequently removed with 4 M HCl

at room temperature to provide target compounds **7a–g** as hydrochloride salts.

The diimides compounds **9b–g** and **11e–g** were synthesized following a similar two-step procedure reported in Scheme 2. The naphthalene and biphenyl tetracarboxylic dianhydrides (**2, 3**) were condensed with corresponding amines (**4**) to give **8b–g** and **10e–g**, respectively.[11,28] After purification by flash column chromatography, these intermediates were mixed with 4 M HCl at room temperature to obtain the target compounds (**9b–g, 11e–g**) in the form of hydrochloride salts with a yield between 60% and 80%.

2.2. Growth-Inhibiting Activity. Novel compounds were evaluated by in vitro MTT (3-(4,5-dimethylthiazol-2-yl)-2,5-diphenyltetrazolium bromide) assays for their antiproliferative

Table 1. In Vitro Activity of New Compounds against Four Kinds of Tumor Cell Lines

compd	R_2, X	IC$_{50}$ (μM)[a]			
		HepG2	MDA-MB-231	K562	HCT-116
amonafide	$R_2 = (CH_2)_2N(CH_3)_2$, X = 0	36	42	31.7	32
7a	$R_2 = (CH_2)_2N(CH_3)_2$, X = 1	37.0	39.2	>50	nd[b]
7d	$R_2 = (CH_2)_4NH(CH_2)_4NH_2$, X = 2	17.1	19.2	14.4	nd[b]
7e	$R_2 = (CH_2)_3NH(CH_2)_3NH(CH_2)_3NH_2$, X = 3	15.6	14.6	14.4	nd[b]
7f	$R_2 = (CH_2)_3NH(CH_2)_4NH(CH_2)_3NH_2$, X = 3	15.8	14.5	14.2	nd[b]
7g	$R_2 = (CH_2)_4NH(CH_2)_4NH(CH_2)_4NH_2$, X = 3	32.1	19.1	14.2	nd[b]
9b	$R_2 = (CH_2)_3NH(CH_2)_3NH_2$, X = 4	2.83	2.95	1.01	5.02
9c	$R_2 = (CH_2)_4NH(CH_2)_3NH_2$, X = 4	33.3	20.2	21.2	nd[b]
9d	$R_2 = (CH_2)_4NH(CH_2)_4NH_2$, X = 4	43.8	27.6	41.0	nd[b]
9e	$R_2 = (CH_2)_3NH(CH_2)_3NH(CH_2)_3NH_2$, X = 6	48.5	18.0	21.2	nd[b]
9f	$R_2 = (CH_2)_3NH(CH_2)_4NH(CH_2)_3NH_2$, X = 6	1.22	0.45	nd[b]	0.13
9g	$R_2 = (CH_2)_4NH(CH_2)_4NH(CH_2)_4NH_2$, X = 6	>50	>50	28	nd[b]
11e	$R_2 = (CH_2)_3NH(CH_2)_3NH(CH_2)_3NH_2$, X = 6	>50	>50	nd[b]	>50
11f	$R_2 = (CH_2)_3NH(CH_2)_4NH(CH_2)_3NH_2$, X = 6	>50	>50	nd[b]	nd[b]
11g	$R_2 = (CH_2)_4NH(CH_2)_4NH(CH_2)_4NH_2$, X = 6	>50	>50	nd[b]	>50

[a]IC$_{50}$ values represent the concentration causing 50% growth inhibition. They were determined by the linear regression method. Each sample is the mean of three independent experiments. [b]Not determined.

activity against HCT-116 (human colorectal cancer cell line), K562 (human leukemia cell line), MDA-MB-231 (human breast cancer cell line), and HepG2 (human hepatoma cell line). Amonafide was tested as a reference compound. The structures and biological results of target compounds were shown in Table 1. The polyamine modified monoimides (7c–g) exhibited better cytotoxic activity than amonafide, while 7a, with a simple replacement of 5-amino by 6-phenyl group in amonafide, did not result in biological improvement. On the other hand, all 6-phenyl naphthalimide–polyamine conjugates are less potent in vitro than previously reported naphthalimide–polyamine conjugates.[23,24] Two series of diimide–polyamine conjugates displayed contrary inhibitive behaviors against tested tumor cells. Surprisingly, the biphenyl diimides (11e–g) were nontoxic, whereas naphthalene diimide derivatives exhibited mixed results. Compounds 9b and 9f displayed much improved potency in comparison to the other analogues in this series, which were just as potent as amonafide. 9b and 9f, the most active compounds in the three types of synthesized imide/diimides, were as potent as previously reported naphthalimide–polyamine conjugates.[23,24]

To furnish more comprehensive and credible information about the cytotoxicity produced by the tested compounds, we applied a high content screening (HCS) technique to assess related cytotoxic indicators in the HepG2 cells. HCS can simultaneously monitor these multiple indicators and detect the earliest onset of toxic effects of tested compounds to increase the predictive power of the in vitro assay. Indeed, cytotoxicity is a complicated gradual process in which changes in nuclear morphology, mitochondrial membrane potential, lysosomal mass/pH, and cell membrane permeability could be observed.[29] In the experiments, changes in nuclear morphology are monitored by staining with the nuclear dye Hoechst 33342. Cell membrane permeability changes are measured using a

permeability dye that stains nuclei in permeability compromised cells, giving a green fluorescence. Mitochondrial transmembrane potential changes are measured using a mitochondrial membrane potential dye that accumulates in healthy mitochondria with intact membrane potential and is absent from depolarized mitochondria. Changes in lysosomal mass/pH are measured using a dye that is a weak base and accumulates in lysosomes during cytotoxicity occurs.

Results in Figure 3A corroborated that some typical imide–polyamine derivatives displayed cytotoxicity in HepG2 cell line in vitro. In Figure 3A, after treatment with the most potent compound 9f, cell nuclear shrinkage, membrane permeability augmentation, mitochondrial membrane potential degradation, and lysosomal mass/pH accruement were detected in a dose dependent manner. 7a and amonafide with equivalent IC$_{50}$ values performed similarly in these indicators. No significant changes of these indicators were found in cells treated by less toxic compounds such as 11g.

In Figure 3B, the cytotoxicity of 9f was more powerful than that of amonafide. For example, after treatment with the same dose of 9f and amonafide (10 μM), the green nucleus and red fluorescence of 9f were obviously increased, suggesting that the integrity of cell membrane was broken down and cytolysosome was activated more potently. Furthermore, the green fluorescence of Rh123 in cytoplasm was significantly decreased, indicating that the mitochondria were destroyed and mitochondrial transmembrane potential was lost.

The measured indicators provide useful information about the mitochondrial membrane potential and lysosomal mass change which are valuable preliminary clues for further mechanistic study. For example, the pronounced variation of lysosomal mass/pH triggered by some imide–polyamine conjugates, observed in Qian's report as well, suggested that lysosomes may be the target of these compounds. Interestingly, amonafide affects LMP in HepG2 cells but does not in HeLa
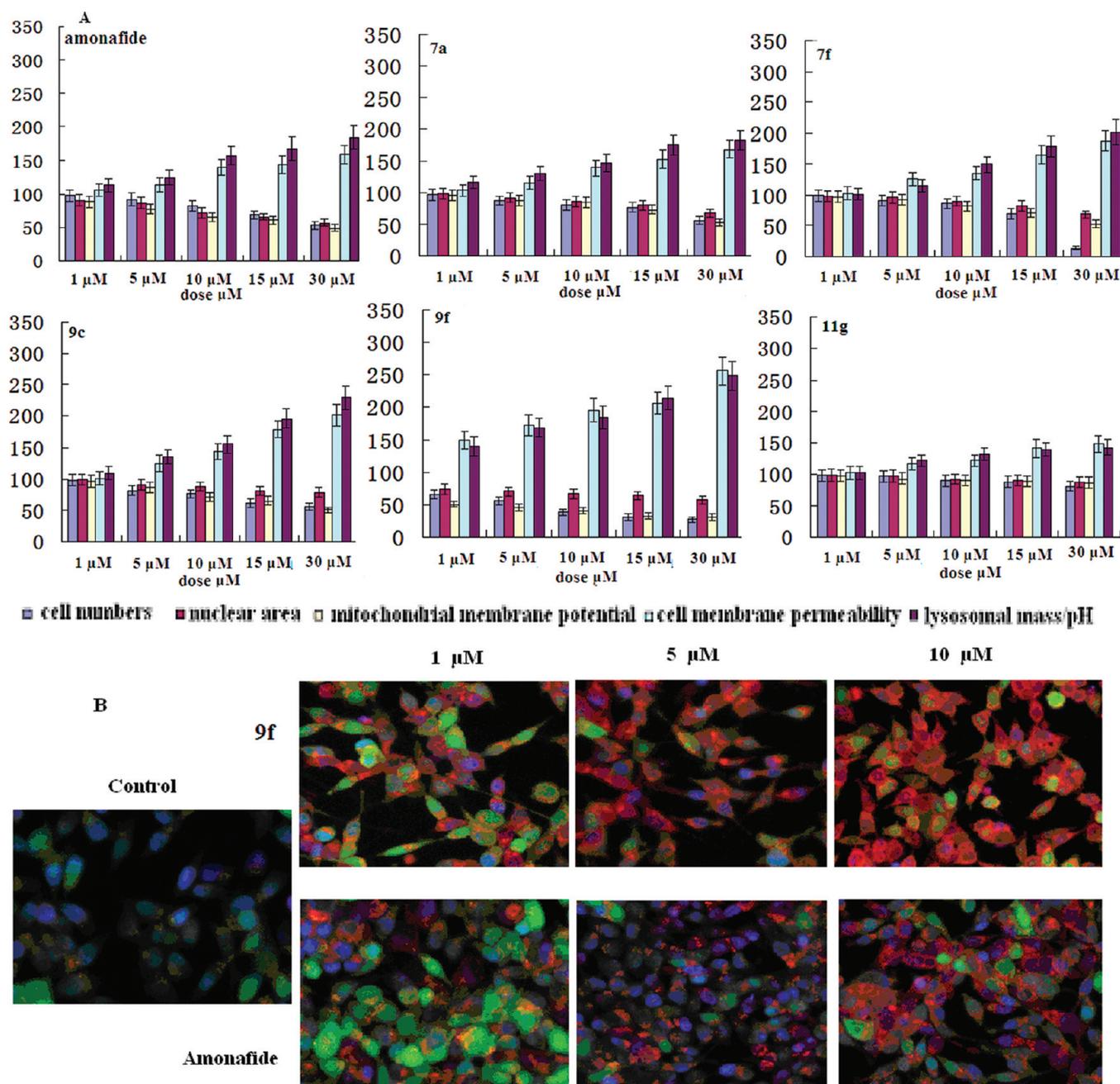
Figure 3. (A) The in vitro cytotoxicity of some new compounds was evaluated in HepG2 cell line after treatment for 48 h. All data are expressed as the mean ± SD from three separate determinations. (B) Representative images showing simultaneous monitoring of changes in cytotoxic indicators. Changes in mitochondrial transmembrane potential (green cytoplasm), cell membrane permeability (green nucleus), nuclear morphology (blue), and lysosomal mass/pH (red) were measured in HepG2 cells after treatment with **9f** or amonafide for 48 h. The cells were imaged using an ArrayScan HCS reader. Scale bar = 10 μm.

cells.[9] On the other side, the changes of mitochondrial membrane potential after drug treatment implied the occurrence of cell apoptosis.

2.3. Apoptosis. Apoptosis or programmed cell death, a favorable ultimate fate of tumor cells, is a complicated cellular process and a major field of interest in antitumor drug development.[30] We and other groups found that naphthalene monoimides and diimides could trigger cell apoptosis.[11,23,24] The above-mentioned MMP changes induced by these newly synthesized naphthalimides suggested that they might produce cytotoxicity through apoptosis. Because of better biological properties, **9f** was chosen for further investigation.

Double staining of HepG2 cells with FITC-labeled annexin V and propidium iodide (PI) was used to illustrate the drug-induced apoptosis. In apoptotic cells, the membrane phospholipid phosphatidylserine (PS) is translocated from the inner to the outer leaflet of the plasma membrane, thereby exposing PS to the external cellular environment. Annexin V, a Ca^{2+} dependent phospholipid-binding protein that has a high affinity for PS, can bind to cells with exposed PS. Annexin V may be conjugated to fluorochromes such as FITC. This format retains its high affinity for PS and thus serves as a sensitive probe for the analysis of cells that are undergoing apoptosis. Since externalization of PS appears in the earlier stages of
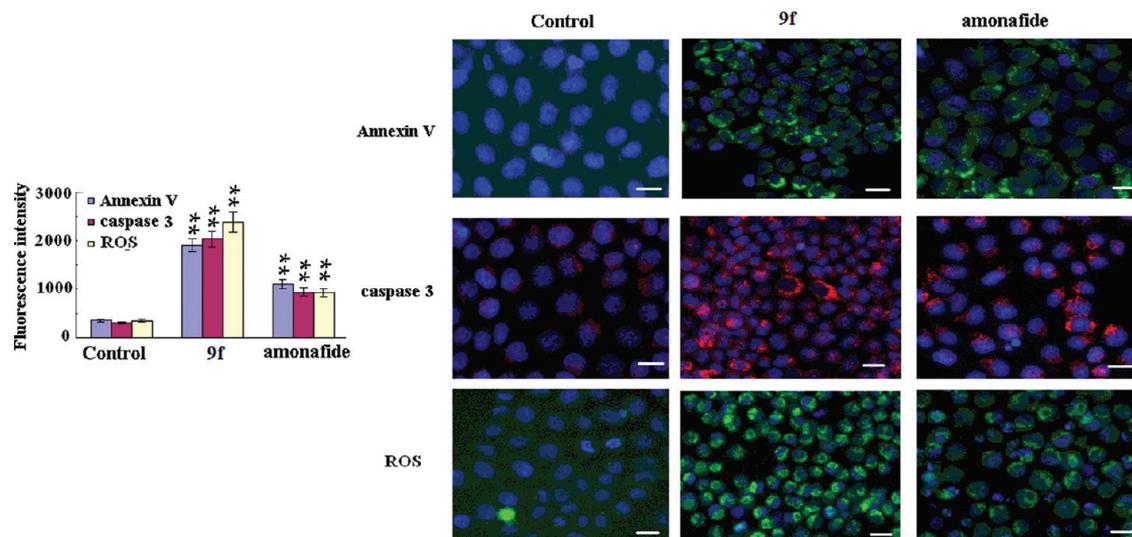
Figure 4. After treatment with **9f** (10 μM) or amonafide (10 μM), annexin V−FITC/PI double staining and caspase activation for apoptosis evaluation and DCFH-DA staining for ROS assay were detected using HCS in HepG2 cells. Images were acquired on the ArrayScan HCS reader using Cellomics' Target Activation BioApplication: scale bar = 10 μm; compared with control, (∗∗) $p < 0.01$.

apoptosis, annexin V−FITC staining can identify apoptosis at an earlier stage. Viable cells with intact membranes exclude PI, whereas the membranes of dead and damaged cells are permeable to PI and the PI bind to cellular DNA. This assessment can distinguish cell apoptosis from necrosis.

Caspase 3 is one of the key proteases in early apoptosis, and it is known that naphthalimides could lead to caspase-dependent apoptosis.[31] Therefore, the activation of caspase 3 was measured by indirect immunofluorescence, using primary antibody against the cleaved portions of caspase 3.

We previously reported that significant reactive oxygen species (ROS) accumulation triggered by MNISpd is closely related to polyamine oxidase (PAO) activity.[25] Destabilization of the lysosome has recently been linked to cytotoxicity involving ROS generation and associated disruption of mitochondrial membrane potential.[32] On the basis of the above-mentioned results, ROS generation was measured by the DCFH-DA (2′,7′-dichlorodihydrofluorescein diacetate) method as well.

As shown in Figure 4, after incubation for 48 h, both **9f** and amonafide did induce HepG2 cell apoptosis, supported by the significant variation of annexin V, accompanied by a pronounced generation of ROS and an increase in caspase 3 activation as evidenced by the staining of active (cleaved) caspase 3. At the same concentration, **9f** could lead to more obvious variations in three detected indexes than amonafide. These initial data suggested that this apoptosis is triggered via a ROS-mediated mitochondrial pathway.[25,33]

Tumiatti et al. also found that some naphthalene diimides and the reference drug mitonafide (similar to amonafide in which the 5-NH$_2$ is replaced by 5-NO$_2$) activate caspase 3 and trigger human HL60 leukemia cells apoptosis.[11] Interestingly, the detailed reports by Kiss et al. revealed that UNBS3157 and UNBS5162, the 5-urea substituted mononaphthalimide derivatives, exert antitumor effects via nonapoptotic manner, which is evidently different from that of amonafide.[8,34] For example, 10 μM UNBS5162 (a hydrolyzed product of UNBS3157) does not trigger apoptosis but induces autophagy and senescence in tested human DU-145 prostate cancer cells.[34] Thus, even for drugs of the same class, their effect on cell proliferation and cell death may be diverse and is perhaps associated with minor structural variation, cell type, and drug concentration, etc.

2.4. Antitumor Activity in Vivo. As an emerging field of polyamine, drug−polyamine conjugates that reinforce the efficacy of vectored drug in addition to the inhibition of polyamine cycle have attracted more attention.[16−18] However, few in vivo studies provided limited messages for rational design of the conjugates in comparison to the plentiful in vitro data. Indeed, in vivo and in vitro experiments may give contradictory information in many cases. The excellent in vitro impacts are often not translated into expected potency in vivo. Therefore, the criteria of lead compounds should include the in vivo trials which may be more important than in vitro ones. To further evaluate the antitumor activity of **9f** in vivo, we chose three H22 (mice hepotoma cell line) tumor transplant models: solid tumor (tumor growth inhibition evaluation), ascites tumor (live time evaluation), and pulmonary metastasis tumor (tumor metastasis evaluation). We compared the antitumor effect of **9f** with amonafide in the H22 subcutaneous model. The 5×10^6 H22 cells were inoculated into 30 female Kunming mice to establish an H22 cancer model, and the treatments were randomized into three groups (n = 10 mice per group): **9f** group, positive control group, negative control group. The first group was injected intravenously everyday with **9f** (0.2 mg/kg) from the day of inoculation, and the second treatment group was injected everyday with amonafide (5 mg/kg) as the positive control group. The third group was injected everyday with normal saline as negative control group. The tumor growth inhibition rates of each group were calculated, and the ratios are 51.8% ((0.68 ± 0.29) g) and 44.7% ((0.78 ± 0.27) g) for **9f** and amonafide compared to the control mice ((1.41 ± 0.18) g), respectively (Figure 5A and Figure 5B). Thus, tumor growth inhibitory rates in mice treated with **9f** and amonafide were dramatically decreased, and the in vitro antitumor effect of **9f** was slightly stronger than that of amonafide. Pathologic examination (HE staining) demonstrated that the survival cells were more obviously dropped after treatment with **9f** than amonafide (Figure 5C).

The impacts of **9f** on survival time in H22-bearing mice were evaluated by measuring the extension of the lifespan. The median survival time (MST) in the control mice was (12.7 ±
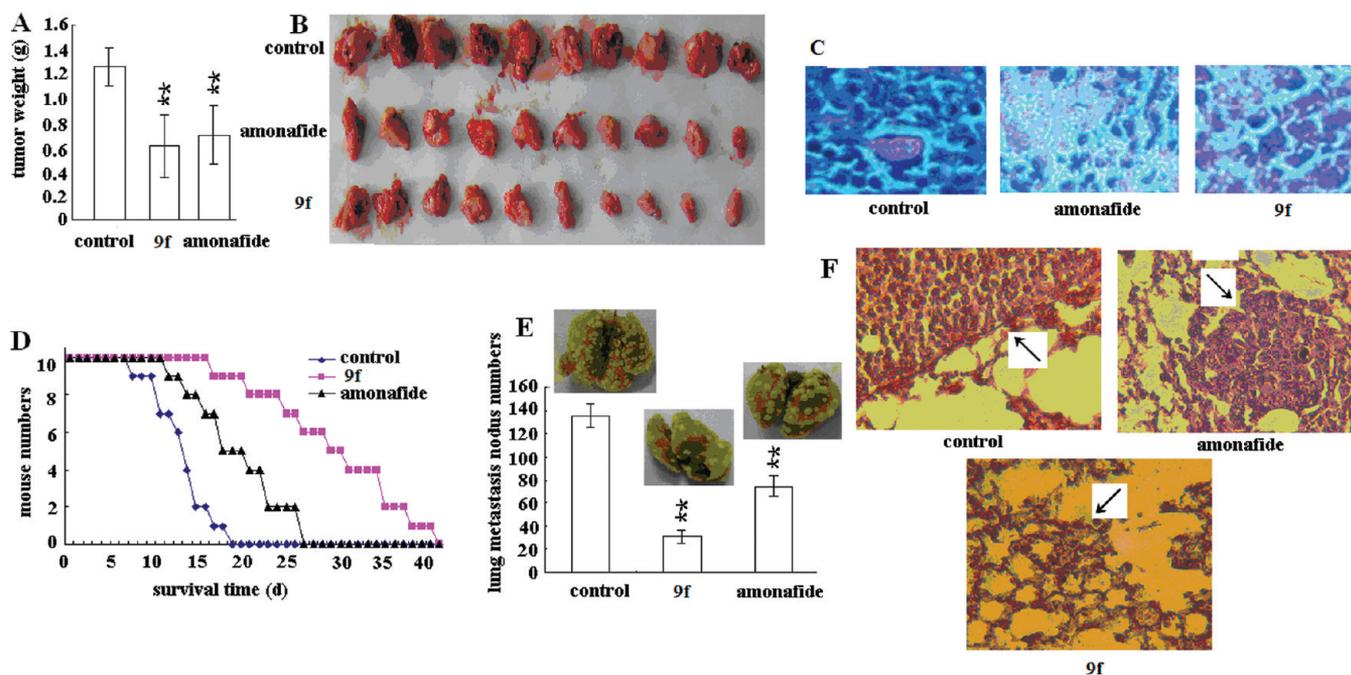
Figure 5. Antitumor activity of **9f** was evaluated in vivo. (A) Mean tumor weight in subcutaneous model, compared with control: (∗∗) $p < 0.01$, $n = 10$. (B) Photographs of tumor were obtained from each treatment group excised on day 10. (C) Representative photograph of histological section was obtained from each treatment group excised on day 10 (HE stain, ×20). (D) Kaplan−Meier curves showing survival of mice treated with **9f** (red), amonafide (black), and normal saline (blue). (E) Antitumor effect of **9f** in the H22 hepatoma pulmonary metastasis model. Photograph (up) and lung metastasis nodus numbers (down) are shown for pulmonary metastasis in mice treatment with **9f**, amonafide, and normal saline. (F) Representative lung metastasis photograph of histological section was obtained from each treatment group (HE stain, ×20): arrow, lung metastasis.

2.5) days. After the **9f** or amonafide was iv administrated, the lifespan was increased by 2.3-fold ((29.8 ± 4.4) days) or 1.5-fold ((18.9 ± 3.6) days) compared with that of the control group, respectively (Figure 5D)

The tumor metastasis is fatal to many patients. On the basis of the versatile characters of polyamines, we hypothesized that polyamines may endow extra functions to parent drugs, and thus, the polyamine conjugates may have broad antitumor spectra. To test whether **9f** was effective against an established lung metastasis, we injected H22 cells intravenously into 30 Kunming mice (5×10^6 cells each mouse). To ensure that all mice bore actively growing lung tumors before the drug treatment, pulmonary cancer was allowed to develop for 10 days. After establishment of tumors, the mice (10 in each treatment group) were injected intravenously on day 11 with **9f** (0.2 mg/kg), amonafide (5 mg/kg, positive control), and normal saline (negative control) for 7 consecutive days. On day 18, mice treated with **9f** displayed few or no visible metastases, whereas all mice treated with normal saline had an extensive tumor burden in the lungs. In contrast, amonafide moderately decreased lung metastasis nodus numbers (Figure 5E). Furthermore, pathologic examination (HE staining) also confirmed that the metastasis focuses were obviously decreased after treatment with **9f** than amonafide (Figure 5F).

The inhibitory effect on metastasis could also be reflected in a statistically marked reduction in tumor weight in the lung on day 18 compared with control. The mean values were 0.17 ± 0.08 g for mice treated with 0.2 mg/kg **9f**, 0.29 ± 0.11 g for mice treated with 5 mg/kg amonafide, and 0.34 ± 0.15 g for mice treated with normal saline. These results supported that **9f** inhibited the tumor metastasis more potently than amonafide.

2.5. Systemic Toxicity. It is reported that amonafide can result in severe irreversible hematotoxicity, which greatly limits its clinical application.[35] In both cell and animal models, some polyamine conjugates such as F14512 have been confirmed to possess favorable cell or tissue selectivity,[19] which is expected to reduce the adverse effects of parent drugs. However, there are few reports about the systemic toxicology of naphthalimide−polyamine conjugates to support the above hypothesis. Consequently, we appraised the systemic toxicity of **9f** (0.2 mg/kg) with amonafide (5 mg/kg) in tumor-bearing mice for 7 consecutive days (intravenous injection). At the same time, the body weight was monitored to detect the dose-limited toxicity. On day 8, these mice were killed by cervical vertebra, and the organs and tissues, including samples of blood, brain, heart, liver, lung, kidney, spleen, thymus, and bone marrow, were taken for inspection of systemic toxicity. We did not observe any weight loss in the **9f**-treated mice, whereas treatment with amonafide was associated with some weight loss, indicating possible dose-limited toxicity (Figure 6A). **9f** also did not lead to significant drops in platelet, red blood cell, and white blood cell numbers compared to controls, while amonafide did. Furthermore, **9f** did not obviously influence bone marrow cell numbers, which is one of the main adverse effects of amonafide, suggesting that **9f** had no hematotoxicity in this test (Figure 6B). The spleen and thymus index number had no significant variation after **9f** treatment compared to controls, whereas amonafide obviously decreased these index numbers, implying that **9f** had no influence on immune function and amonafide inhibited immune function to some extent (Figure 6C). Heart, liver, kidney, brain, lung, and spleen had no pathological changes in the pathology examination of both compounds (Figure 6D and Figure 6E). In short, **9f** performed better than
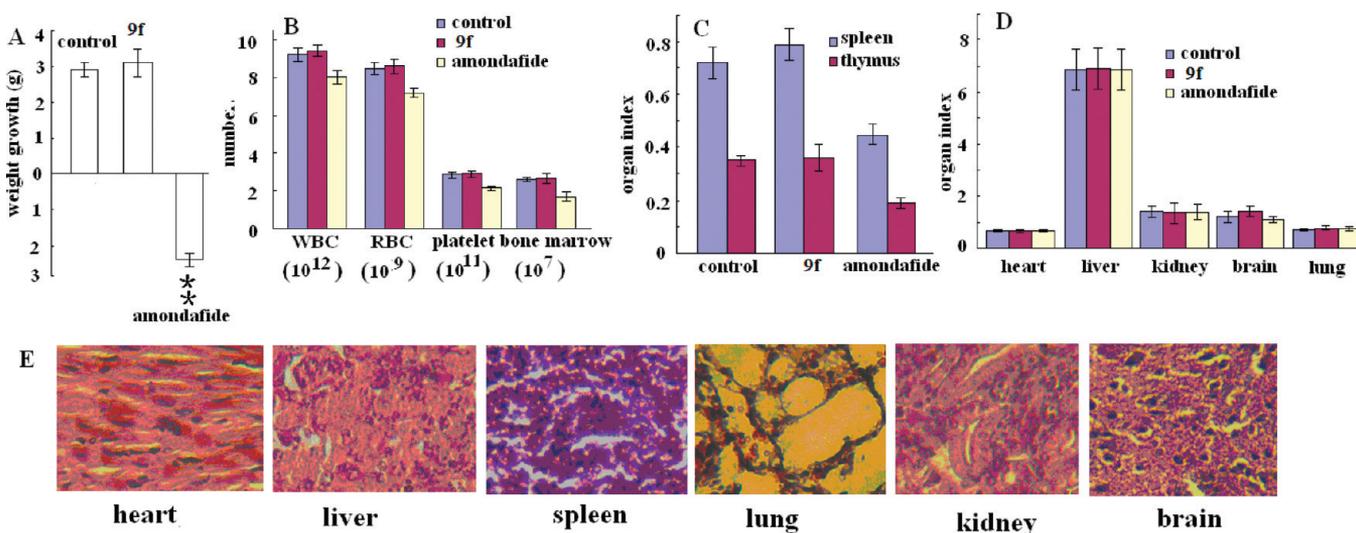
Figure 6. Systemic toxicity of **9f**. (A) The mean weight change was shown after treatment with **9f**, amonafide, and normal saline: compared with control, (∗∗) $p < 0.01$, $n = 10$. (B) The hematotoxicity was evaluated after treatment with **9f**, amonafide, and normal saline. (C) The immune organs (spleen and thymus) were evaluated after treatment with **9f**, amonafide, and normal saline. (D) The organ index (heart, liver, kidney, brain, and lung) was evaluated after treatment with **9f**, amonafide, and normal saline. (E) Representative photograph of histological section was obtained from each treatment group (HE stain, 20×).

amonafide in the experiments of toxicological profile at the doses that exert antitumor activity in vivo.

It is interesting to compare the results of **9f** with UNBS3157 and UNBS5162. To alleviate the toxicity of amonafide, Kiss et al. transformed the aryl 5-amino group to 5-urea motif to prevent its metabolization to *N*-acetylamonafide by the enzyme *N*-acetyltransferase 2. Indeed, the synthesized UNBS3157 and its hydrolyzed product UNBS5162 are nonhematotoxic.[8,34] As for **9f** with primary amino groups in polyamine skeletons but without amino group in the aryl system, the observed non-hematotoxicity at the therapeutic dose implied that the terminal amino groups in the polyamine tails did not display negative functions in the present toxicological assays.

3. CONCLUSION

Three series of aromatic imide/diimides modified polyamines were synthesized, and their antitumor activities were evaluated in vitro and in vivo. Both the imide/diimides scaffold and the polyamine motif affect the biological activity of designed compounds. Two naphthalene diimide−polyamine conjugates more potently inhibited the growth of multiple cancer cell lines than the reference drug amonafide. **9f**, which was tested more comprehensively as a representative candidate, was verified to efficiently induce apoptosis via a ROS mediated mitochondrial pathway in the preliminary study of cell death profile. The in vivo trials of H22 tumor transplant models revealed that **9f** expressed improved indexes of inhibitive effect and lifespan extension compared to amonafide. The dropped hematotoxicity, which is one of main drawbacks of amonafide, testified that **9f** is a valuable lead compound for further investigation. More importantly, the obviously improved ability of **9f** in preventing lung cancer metastasis was observed, which increased its value as a promising lead compound. Present experiments again indicated that the polyamine motifs may enhance the antitumor efficacy and alleviate the adverse effects of vectored drugs in certain cancerous models. In addition, the versatile function of polyamines may endow some unexpected biological behaviors to the parent drugs. Compared to the extensive study of apoptotic mechanism, the signaling pathway of inhibiting metastasis by naphthalimides is rarely reported, which is underway in our laboratory.

4. EXPERIMENTAL PROTOCOLS

4.1. Synthesis of Aromatic Imide and Diimide−Polyamine Conjugates. All solvents and reagents were purchased from the suppliers and used without further purification. All ¹H NMR spectra were recorded on a Bruker AV-400 model spectrometer in D_2O or $CDCl_3$. Chemical shifts for ¹H NMR spectra are reported in parts per million to residual solvent protons. ESI-MS spectra were recorded on an ESQUIRE-LC mass spectrometer. The target compounds with the purity being higher than 95% were analyzed using combustion analysis. Elemental analyses were performed on a Gmbe VarioEL elemental instrument, and results were within 0.4% of the theoretical values.

4.1.1. General Procedure for the Synthesis of 6a,d−g. A mixture of 4-bromo-1,8-naphthalic anhydride and polyamine (in a 1:1 molar ratio) in EtOH was heated at refluxing temperature, and the reaction process was monitored by TLC. After completion, the reaction mixture was cooled to room temperature and concentrated under vacuum to give an oily residue, which was further purified to obtain the BOC protected intermediates **5a,d−g**.

A 50 mL round bottomed flask equipped with a magnetic stirring bar was charged with pure **5** (2 mmol), phenylboronic acid (2 mmol), K_2CO_3 (3 mmol), a catalytic amount of $PdCl_2$, and tetrabutylammonium bromide. The mixture was vigorously stirred for 6 h at the boiling temperature. After reaction completion, the reaction mixture was filtered and evaporated to dryness, and the residue was subjected to column chromatography using ethyl acetate/petroleum ether mixture as the eluent to yield the compounds **6a,d−g**.

2-[(2-Dimethylamino)ethyl]-6-phenyl-1H-benz[de]isoquinoline-1,3(2H)-dione (6a). Yield 84%, white solid. ¹H NMR (400 MHz, $CDCl_3$) δ: 8.62 (t, J = 6.4 Hz, 2H, Ar-H); 8.25 (d, J = 8.4 Hz, 1H, Ar-H); 7.66−7.70 (m, 2H, Ar-H); 7.48−7.56 (m, 5H, Ar-H); 4.35 (t, J = 7.2 Hz, 2H, 1 × N-CH₂), 2.67 (t, J = 7.2 Hz, 2H, 1 × N-CH₂); 2.36 (s, 6H, 2 × N-CH₃). ESI-MI *m/z*: 345.1 [M + 1]⁺.

2-[4-(4-Butoxycarbonylaminobutylbutoxycarbonylamino)butyl]-6-phenyl-1H-benz[de]isoquinoline-1,3(2H)-dione (6d). Yield 85%, pale yellow oil. ¹H NMR (400 MHz, $CDCl_3$) δ: 8.55 (t, J = 6.8 Hz, 2H, Ar-H); 8.19 (d, J = 8.4 Hz, 1H, Ar-H); 7.62 (t, J = 6.2 Hz, 2H, Ar-H); 7.43−7.51 (m, 5H, Ar-H); 4.16 (t, J = 7.0 Hz, 2H, 1 × N-CH₂); 3.08−3.19 (m, 6H, 3 × N-CH₂); 1.67−1.74 (m, 2H, 1 × CH₂); 1.60−1.62 (m,

2H, 1 × CH$_2$); 1.47–1.54 (m, 2H, 1 × CH$_2$); 1.39–1.44 (m, 20H, 1 × CH$_2$ + 6 × CH$_3$). ESI-MI m/z: 638.3 [M + Na]$^+$.

2-{3-[3-(3-Butoxycarbonylaminopropylbutoxycarbonylamino)-propylbutoxycarbonylamino]propyl}-6-phenyl-1H-benz[de]isoquinoline-1,3(2H)-dione (6e). Yield 86%, pale yellow oil. ^{1}H NMR (400 MHz, CDCl$_3$) δ: 8.53–8.55 (m, 2H, Ar-H); 8.19 (d, 1H, J = 7.2 Hz, Ar-H); 7.61 (s, 2H, Ar-H); 7.42–7.50 (m, 5H, Ar-H); 4.14 (t, J = 7.8 Hz, 2H, 1 × N-CH$_2$); 3.04–3.32 (m, 10H, 5 × N-CH$_2$); 1.91–1.97 (m, 2H, 1 × CH$_2$); 1.59–1.69 (m, 2H, 1 × CH$_2$); 1.36–1.46 (m, 29H, 1 × CH$_2$ + 9 × CH$_3$). ESI-MI m/z: 767.4 [M + Na]$^+$.

2-{3-[4-(3-Butoxycarbonylaminopropylamino)-butylbutoxycarbonylamino]propyl}-6-phenyl-1H-benz[de]isoquinoline-1,3(2H)-dione (6f). Yield 83%, pale yellow oil. ^{1}H NMR (400 MHz, CDCl$_3$) δ: 8.63 (t, J = 6.6 Hz, 2H, Ar-H); 8.27 (d, 1H, J = 8.4 Hz, Ar-H); 7.69 (t, J = 7.2 Hz, 2H, Ar-H); 7.49–7.57 (m, 5H, Ar-H); 4.20–4.23 (t, J = 6.4 Hz, 2H, 1 × N-CH$_2$); 3.09–3.39 (m, 10H, 5 × N-CH$_2$); 1.95–2.03 (m, 2H, 1 × CH$_2$); 1.63–1.64 (m, 2H, 1 × CH$_2$); 1.42–1.50 (m, 31H, 2 × CH$_2$ + 9 × CH$_3$). ESI-MI m/z: 781.4 [M + Na]$^+$.

2-{4-[4-(4-Butoxycarbonylaminobutylbutoxycarbonylamino)-butylbutoxycarbonylamino]butyl}-6-phenyl-1H-benz[de]isoquinoline-1,3(2H)-dione (6g). Yield 86%, pale yellow oil. ^{1}H NMR (400 MHz, CDCl$_3$) δ: 8.56–8.66 (m, 3H, Ar-H); 8.40 (d, 1H, J = 7.6 Hz, Ar-H); 8.04 (t, J = 8.0 Hz, 1H, Ar-H); 7.83–7.87 (m, J = 8.0 Hz, 1H, Ar-H); 7.68–7.73 (m, 1H, Ar-H), 7.49–7.57 (m, 3H, Ar-H); 4.18 (t, J = 7.2 Hz, 2H, 1 × N-CH$_2$); 3.13–3.15 (m, 10H, 5 × N-CH$_2$); 1.62–1.72 (m, 6H, 3 × CH$_2$); 1.41–1.46 (m, 33H, 3 × CH$_2$ + 9 × CH$_3$). ESI-MI m/z: 809.5 [M + Na]$^+$.

4.1.2. General Procedure for the Synthesis of 7a,d–g. The respective N-Boc protected intermediates 7a–g (1.2 mmol) were dissolved in EtOH (20 mL) and stirred at 0 °C for 10 min. Then 4 M HCl was added dropwise at 0 °C. The reaction mixture was stirred at room temperature overnight. (After 0.6 mL of 4 M HCl is added, the mixture was stirred for 30 min for 7a.) The solution typically gave a white solid as a precipitate. The solid was filtered, washed several times with absolute ethanol, and dried under vacuum to give the pure target compounds 7a,d–g.

2-[(2-Dimethylamino)ethyl]-6-phenyl-1H-benz[de]isoquinoline-1,3(2H)-dione Hydrochloride (7a). Yield 80%, white solid. ^{1}H NMR (400 MHz, D$_2$O) δ: 8.59 (t, J = 6.2 Hz, 2H, Ar-H); 8.22 (d, J = 8.4 Hz, 1H, Ar-H); 7.66 (t, J = 6.8 Hz, 2H, Ar-H); 7.45–7.53 (m, 5H, Ar-H); 4.33 (t, J = 7.0 Hz, 2H, 1 × N-CH$_2$), 2.66 (t, J = 6.8 Hz, 2H, 1 × N-CH$_2$); 2.35 (s, 6H, 2 × N-CH$_3$). ESI-MI m/z: 345.1 [M + 1 – HCl]$^+$. Anal. Calcd for C$_{22}$H$_{21}$N$_2$O$_2$Cl·0.25H$_2$O: C 68.57%, H 5.62%, N 7.27%. Found: C 68.65%, H 5.92%, N 7.28%.

2-[4-(4-Aminobutylamino)butyl]-6-phenyl-1H-benz[de]isoquinoline-1,3(2H)-dione Dihydrochloride (7d). Yield 83%, white solid. ^{1}H NMR (400 MHz, D$_2$O) δ: 7.74 (d, J = 7.2 Hz, 1H, Ar-H); 7.53–7.58 (m, 2H, Ar-H); 7.37–7.44 (m, 3H, Ar-H); 7.04 (t, J = 7.0 Hz, 1H, Ar-H); 6.94 (d, J = 6.8 Hz, Ar-H); 6.79 (d, J = 7.6 Hz, 1H,Ar-H); 3.61 (t, J = 6.6 Hz, 2H, 1 × N-CH$_2$); 3.06–3.13 (m, J = 7.8 Hz, 4H, 2 × N-CH$_2$); 3.02 (t, J = 8.0HZ, 2H, 1 × N-CH$_2$); 1.78–1.83 (m, 4H, 2 × CH$_2$); 1.65–1.73 (m, 2H,1 × CH$_2$); 1.37–1.42 (m, 2H, 1 × CH$_2$). ESI-MI m/z: 416.3 [M + H – 2HCl]$^+$. Anal. Calcd for C$_{26}$H$_{31}$Cl$_2$N$_3$O$_2$·1.8H$_2$O: C 59.95%, H 6.70%, N 8.07%. Found: C 59.63%, H 6.33%, N 8.09%.

2-{3-[3-(3-Aminopropylamino)propylamino]propyl}-6-phenyl-1H-benz[de]isoquinoline-1,3(2H)-dione Trihydrochloride (7e). Yield 82%, white solid. ^{1}H NMR (400 MHz, D$_2$O) δ: 7.79 (d, J = 6.8 Hz, 1H, Ar-H); 7.64 (d, J = 6.8 Hz, 1H, Ar-H); 7.53 (d, 1H, J = 8.4 Hz, Ar-H); 7.30–7.37 (m, 3H, Ar-H); 7.05 (t, J = 6.8 Hz, 1H, Ar-H); 6.90 (d, J = 6.4 Hz, 2H, Ar-H); 6.81 (d, J = 7.2 Hz, 1H, Ar-H); 3.74 (t, 2H, 1 × N-CH$_2$); 3.06–3.16 (m, 10H, 5 × N-CH$_2$); 2.01–2.14 (m, 2H, 1 × CH$_2$); 1.87–1.89 (m, 2H, 1 × CH$_2$); 1.71–1.76 (m, 2H, 1 × CH$_2$). ESI-MI m/z: 445.3 [M + H – 3HCl]$^+$. Anal. Calcd for C$_{27}$H$_{35}$Cl$_3$N$_4$O$_2$·1.5H$_2$O: C 55.82%, H 6.59%, N 9.64%. Found: C 55.62%, H 6.67%, N 9.68%.

2-{3-[4-(3-Aminopropylamino)butylamino]propyl}-6-phenyl-1H-benz[de]isoquinoline-1,3(2H)-dione Trihydrochloride (7f). Yield 84%, white solid. ^{1}H NMR (400 MHz, D$_2$O) δ: 7.88 (d, J = 7.2 Hz, 1H, Ar-H); 7.74 (d, J = 7.6 Hz, 1H, Ar-H); 7.58 (d, J = 8.4 Hz, 1H, Ph-H); 7.34–7.43 (m, 3H, Ar-H); 7.11 (t, J = 7.0 Hz, 1H, Ar-H); 6.94 (d, J = 7.2 Hz, 2H, Ar-H); 6.87 (d, J = 7.6 Hz, 1H, Ar-H); 3.85 (t, J = 6.0 Hz, 2H, 1 × N-CH$_2$); 3.14–3.26 (m, 10H, 5 × N-CH$_2$); 2.13–2.21 (m, 2H, CH$_2$); 1.95–2.02 (m, 2H, 1 × CH$_2$); 1.87–1.89 (m, 4H, 2 × CH$_2$). ESI-MI m/z: 459.3 [M + H – 3HCl]$^+$. Anal. Calcd for C$_{28}$H$_{37}$O$_2$N$_4$Cl$_3$·0.5H$_2$O: C 58.29%, H 6.64%, N 9.71%. Found: C 58.09%, H 6.47%, N 9.81%.

2-{4-[4-(4-Aminobutylamino)butylamino]butyl}-6-phenyl-1H-benz[de]isoquinoline-1,3(2H)-dione Trihydrochloride (7g). Yield 82%, white solid. ^{1}H NMR (400 MHz, D$_2$O) δ: 7.58 (d, J = 6.4 Hz, 1H, Ar-H); 7.21–7.36 (m, 5H, Ar-H); 6.82–6.84 (m, 1H, Ar-H); 6.74 (d, J = 5.6 Hz, 2H, Ar-H); 6.51 (d, J = 6.0 Hz, 1H, Ar-H); 3.48 (t, J = 2.8 Hz, 2H, 1 × N-CH$_2$); 2.95–3.08 (m, 10H, 5 × N-CH$_2$); 1.73–1.76 (m, 8H, 4 × CH$_2$); 1.62–1.63 (m, 2H, 1 × CH$_2$); 1.23–1.29 (m, 2H, 1 × CH$_2$). ESI-MI m/z: 487.4 [M + H – 3HCl]$^+$. Anal. Calcd. for C$_{30}$H$_{41}$Cl$_3$N$_4$O$_2$·0.5H$_2$O: C 59.55%, H 7.00%, N 9.26%. Found: C 59.77%, H 7.32%, N 9.07%.

4.1.3. General Procedure for the Synthesis of 9b–g and 11e–g. A mixture of the respective dianhydride and polyamine (in a 1:1 molar ratio) in the solvents EtOH and toluene (v:v = 1:1) was heated at refluxing temperature and monitored by TLC. After completion, the reaction mixture was cooled to room temperature and concentrated under vacuum to give an oily residue, which was further purified to obtain the BOC protected intermediates 8b–g (10e–g).

Target compounds 9b–g (11e–g) were obtained in the same way as described in the synthesis of 7a–g.

2,7-Bis[3-(3-aminopropylamino)propyl]benzo[lmn][3,8]-phenanthroline-1,3,6,8(2H,7H)-tetraone Tetrahydrochloride (9b). Yield 83%, white solid. ^{1}H NMR (400 MHz, D$_2$O) δ: 8.45 (S, 4H, Ar-H); 4.22 (t, J = 6.8 Hz, 4H, 2 × N-CH$_2$); 3.20–3.27 (m, 8H, 4 × N-CH$_2$); 3.14 (t, J = 7.8 Hz, 4H, 2 × N-CH$_2$); 2.11–2.21 (m, 4H, 2 × CH$_2$). ESI-MI m/z: 495.3 [M + – 4HCl]$^+$. Anal. Calcd for C$_{26}$H$_{38}$Cl$_4$N$_6$O$_4$·2H$_2$O: C 46.16%, H 6.26%, N 12.42%. Found: C 46.33%, H 6.56%, N 12.65%.

2,7-Bis[4-(3-aminopropylamino)butyl]benzo[lmn][3,8]phenanthroline-1,3,6,8(2H,7H)-tetraone Tetrahydrochloride (9c). Yield 80%, white solid. ^{1}H NMR (400 MHz, D$_2$O) δ: 8.28 (S, 4H, Ar-H); 4.07 (t, J = 7.0 Hz, 4H, 2 × N-CH$_2$); 3.22 (t, J = 7.8 Hz, 8H, 4 × N-CH$_2$); 3.15 (t, J = 7.0 Hz, 4H, 2 × N-CH$_2$); 2.10–2.18 (m, 4H, 2 × CH$_2$); 1.82–1.89 (m, 8H, 4 × CH$_2$). ESI-MI m/z: 523.3 [M + H – 4HCl]$^+$. Anal. Calcd for C$_{28}$H$_{42}$Cl$_4$N$_6$O$_4$·1.5H$_2$O: C 48.35%, H 6.52%, N 12.08%. Found: C 48.09%, H 6.70%, N 11.86%.

2,7-Bis[4-(4-aminobutylamino)butyl]benzo[lmn][3,8]phenanthroline-1,3,6,8(2H,7H)-tetraone Tetrahydrochloride (9d). Yield 83%, white solid. ^{1}H NMR (400 MHz, D$_2$O) δ: 8.32 (S, 4H, Ar-H); 4.09 (t, J = 6.6 Hz, 4H, 2 × N-CH$_2$); 3.15–3.23 (m, 8H, 4 × N-CH$_2$); 3.08 (t, J = 6.8 Hz, 4H, 2 × N-CH$_2$); 1.78–1.84 (m, 16H, 8 × CH$_2$). ESI-MI m/z: 551.4 [M + H – 4HCl]$^+$. Anal. Calcd for C$_{30}$H$_{46}$Cl$_4$N$_6$O$_4$·0.2H$_2$O: C 51.46%, H 6.68%, N 12.00%. Found: C 51.33%, H 6.67%, N 11.82%.

2,7-Bis{3-[3-(3-aminopropylamino)propylamino]propyl}benzo[lmn]-[3,8]phenanthroline-1,3,6,8(2H,7H)-tetraone Hexahydrochloride (9e). Yield 83%, white solid. ^{1}H NMR (400 MHz, D$_2$O) δ: 8.31 (s, 4H, Ar-H); 4.14 (t, J = 6.0 Hz, 4H, 2 × N-CH$_2$); 3.15–3.22 (m, 16H, 8 × N-CH$_2$); 3.09 (t, J = 7.8 Hz, 4H, 2 × N-CH$_2$); 2.04–2.19 (m, 12H, 6 × CH$_2$). ESI-MI m/z: 609.5 [M + H – 6HCl]$^+$. Anal. Calcd for C$_{32}$H$_{54}$Cl$_6$N$_8$O$_4$·1.5H$_2$O·C$_2$H$_5$OH: C 45.34%, H 7.05%, N 12.44%. Found: C 45.45%, H 7.22%, N 12.15%.

2,7-Bis{3-[4-(3-aminopropylamino)butylamino]propyl}benzo[lmn]-[3,8]phenanthroline-1,3,6,8(2H,7H)-tetraone Hexahydrochloride (9f). Yield 82%, white solid. ^{1}H NMR (400 MHz, D$_2$O) δ: 8.57 (s, 4H, Ar-H); 4.28 (t, J = 6.4 Hz, 4H, 2 × N-CH$_2$); 3.15–3.29 (m, 20H, 10 × N-CH$_2$); 2.12–2.24 (m, 8H, 4 × CH$_2$); 1.87 (br s, 8H, 4 × CH$_2$). ESI-MI m/z: 637.5 [M + H – 6HCl]$^+$. Anal. Calcd for C$_{34}$H$_{58}$Cl$_6$N$_8$O$_4$·0.5H$_2$O: C 47.23%, H 6.88%, N 12.96%. Found: C 47.08%, H 6.78%, N 12.74%.

2,7-Bis[4-[4-(4-aminobutylamino)butylamino]butyl}benzo[lmn][3,8]-phenanthroline-1,3,6,8(2H,7H)-tetraone Hexahydrochloride (9g). Yield 82%, white solid. ^{1}H NMR (400 MHz, D$_2$O) δ: 8.24 (s, 4H, Ar-H); 4.04 (t, J = 6.2 Hz, 4H, 2 × N-CH$_2$); 3.14–3.24 (m, 16H, 8 × N-

CH$_2$); 3.09 (t, J = 6.8 Hz, 4H, 2 × N-CH$_2$); 1.80−1.87 (m, 24H, 12 × CH$_2$). ESI-MI m/z: 693.5 [M + H − 6HCl]$^+$. Anal. Calcd for C$_{38}$H$_{66}$Cl$_6$N$_8$ O$_4$·1H$_2$O: C 49.09%, H 7.37%, N 12.05%. Found: C 49.18%, H 7.38%, N 11.93%.

2,2'-Bis{3-[3-(3-aminopropylamino)propylamino]propyl}-5,5'-biisoindoline-1,1',3,3'-tetraone Hexahydrochloride (11e). Yield 83%, white solid. ^{1}H NMR (400 MHz, D$_2$O) δ: 7.92 (dd, $J_1 = J_2$ = 1.2 Hz, 2H, Ar-H); 7.80 (s, 2H, Ar-H); 7.75 (d, J = 7.6 Hz, 2H, Ar-H); 3.78 (t, J = 6.8 Hz, 4H, 2 × N-CH$_2$); 3.19−3.24 (m, 16H, 8 × N-CH$_2$); 3.13 (t, J = 7.8HZ, 4H, 2 × N-CH$_2$); 2.08−2.20 (m, 12H, 6 × CH$_2$). ESI-MI m/z: 635.4 [M + H − 6HCl]$^+$. Anal. Calcd for C$_{34}$H$_{56}$Cl$_6$N$_8$O$_4$·1H$_2$O: C 46.85%, H 6.71%, N 12.86%. Found: C 46.81%, H 6.69%, N 12.70%.

2,2'-Bis{3-[4-(3-aminopropylamino)butylamino]propyl}-5,5'-biisoindoline-1,1',3,3'-tetraone Hexahydrochloride (11f). Yield 80%, white solid. ^{1}H NMR (400 MHz, D$_2$O) δ: 8.09 (d, J = 8.0 Hz, 2H, Ar-H); 8.04 (s, 2H, Ar-H); 7.93 (d, J = 8.0 Hz, 2H, Ar-H); 3.86 (t, J = 6.6 Hz, 4H, 2 × N-CH$_2$); 2.14−3.27 (m, 20H, 10 × N-CH$_2$); 2.11−2.19 (m, 8H, 4 × CH$_2$); 1.85−1.86 (m, 8H, 4 × CH$_2$). ESI-MI m/z: 663.5 [M + H − 6HCl]$^+$. Anal. Calcd for C$_{36}$H$_{60}$Cl$_6$N$_8$O$_4$·0.85H$_2$O: C 48.21%, H 6.93%, N 12.49%. Found: C 48.51%, H 6.72%, N 12.17%.

2,2'-Bis{4-[4-(4-aminobutylamino)butylamino]butyl}-5,5'-biisoindoline-1,1',3,3'-tetraone Hexahydrochloride (11g). Yield 80%, white solid. ^{1}H NMR (400 MHz, D$_2$O) δ: 8.03 (d, J = 2.4 Hz, 2H, Ar-H); 7.95 (d, J = 4.2 Hz, 2H, Ar-H); 7.86 (d, J = 4.8 Hz, 2H, Ar-H); 3.73 (t, J = 6.4 Hz, 4H, 2 × N-CH$_2$); 3.13 (m, 16H, 8 × N-CH$_2$); 3.06 (m, 4H, 2 × N-CH$_2$); 1.79−1.81 (m, 24H, 12 × CH$_2$). ESI-MI m/z: 719.6 [M + H − 6HCl]$^+$. Anal. Calcd for C$_{40}$H$_{68}$Cl$_6$N$_8$O$_4$·0.5H$_2$O: C 50.75%, H 7.35%, N 11.84%. Found: C 50.62%, H 7.12%, N 11.64%.

4.2. Biological Materials and Methods. *4.2.1. Cell Culture and MTT Assay.* HCT-116 cell line, MDA-MB-231 cell line, K562 cell line, and HepG2 cell line were purchased from Shanghai Institute for Biological Science, Chinese Academy of Science (Shanghai, China) and were supplemented with 1 mM glutamine and 10% or 20% (v/v) FCS. Cells were cultured at 37 °C under a 5% CO$_2$ atmosphere. The antiproliferative ability of compounds was evaluated in HCT-116 cells, MDA-MB-231 cells, K562 cells, and HepG2 cells by the conversion of MTT to a purple formazan precipitate as previously described. Cells were seeded into 96-well plates at 5 × 10^3 cells/well. After 12 h, various concentrations (1, 5, 10, 30, and 50 μM) of compounds were subsequently added and incubated for 48 h. (Note: the cytotoxicity of **9f** was confirmed using 0.1, 1, 10, 30, and 50 μM when the IC$_{50}$ values are less than 1 μM.) The inhibition rate was calculated from plotted results using untreated cells as 100%.

4.2.2. Cytotoxic Assay. The cytotoxicity of compounds was evaluated in HepG2 cells using the multiparameter cytotoxicity 2 kit by High Content Screening (HCS, Cellomics ArrayScan Vti, U.S.). Briefly, cells were seeded into 96-well plates at 5 × 10^3 cells/well. After 12 h, various concentrations (1, 5, 10, 15, and 30 μM) of compounds were subsequently added and incubated for 48 h. Cells were stained according to the manufacturer's protocol. Images were acquired on the ArrayScan HCS reader using Multiparameter Cytotoxicity BioApplication software.

4.2.3. Cellular Apoptotic Evaluation. Cell apoptosis was evaluated by annexin V−FITC apoptosis detection kit and caspase 9 and caspase 3 activation kits using HCS. Briefly, the HepG2 cells were seeded in 24-well plates and exposed to compound **9f** for 48 h, then harvested and stained according to the manufacturer's protocol. Images were acquired on the ArrayScan HCS reader using Target Activation BioApplication software.

4.2.4. ROS Determination. Cellular generation of ROS was determined using oxidation of 2′,7′-dichlorodihydrofluorescein diacetate (DCFH-DA) as previously described. Specifically, culture medium from the wells was removed and replaced with 100 μL of new culture medium containing particles at 100 μg/mL. After 2 h of incubation with nanomaterials, a time sufficient to stimulate intracellular ROS production, the cells were rinsed three times with PBS to remove unbound nanomaterials. The cells were then incubated with 100 μL of H$_2$DCFDA (5 μM in PBS) at 37 °C for 30 min.

Following this, the wells were rinsed twice with PBS to remove excess dye and 200 μL of PBS was added to each well. Fluorescence was measured with excitation at 485 nm and emission at 530 nm using a Tecan Infinite M 200 microplate reader (San Jose, CA) with measurements done in quadruplicate. The fluorescence intensities of treated cells were normalized to untreated controls and plotted as relative fluorescence units (RFUs).

4.2.5. Subcutaneous Xenograft of H22 Cells in Kunming Mice. All animal care and experimentation conformed to the Guide for the Care and Use of Laboratory Animals published by Henan University. For solid tumor development, 30 male Kunming mice (Laboratory Animal Center of Henan, Zhengzhou) aged 5 weeks (weighing 18−22 g) were injected subcutaneously with 2 × 10^6 H22 cells. On the eighth day after inoculation, the mice were randomly divided into three groups (control, **9f** group, and amonafide group) and then were administered by caudal vein injection **9f** (0.2 mg/kg) or amonafide (5 mg/kg, as positive control) or physiologic saline for 7 consecutive days. On day 16, the mice were killed by ether anesthesia, and solid tumors were removed and weighed. The inhibitory rate was calculated as follows: inhibitory rate (%) = [(A − B)/A] × 100, where A was the mean tumor weight of the control group and B was that of the drug treated or positive group. After being weighed, the tumors were fixed in formalin and stained with hematoxylin and eosin.

4.2.6. Survival Time in Mice Bearing H22 Cells. For calculation of the survival time, 30 male Kunming mice were inoculated via intraperitoneal (ip) injection with 1 × 10^6 H22 cells/mouse on day 0 and were randomly divided into three groups. The treatment with **9f** (0.2 mg/kg), amonafide (5 mg/kg), or physiologic saline by caudal vein injection was started 24 h after inoculation for 7 consecutive days. The median survival time (MST) for each group was observed, and the antitumor activity of drug was evaluated by measuring the increase of the lifespan. The extended lifespan rate was calculated as follows: extend rate (%) = (MST$_{treated\ group}$/MST$_{control\ group}$) × 100.

4.2.7. H22 Cells Lung Metastasis Models. H22 cells (5 × 10^6 cells per mouse) for Kunming mice were injected iv through the tail vein for tumor passive metastasis. To ensure all mice bore actively growing lung tumors before the drug treatment, pulmonary metastasis was allowed to develop for 10 days. On day 11, mice were injected intravenously with **9f** (0.2 mg/kg), amonafide (5 mg/kg, positive control), and normal saline (negative control) (n = 10) for 7 consecutive days. On day 18, mice were killed by ether anesthesia and lungs were removed and weighed and then fixed in Bouin's fluid. After the lungs were fixed, lung metastases nodus was numbered.

4.2.8. Systemic Toxicity Evaluation. Mice (10 per group) received **9f** (0.2 mg/kg) and amonfide (5 mg/kg, iv) for 7 consecutive days and then were sacrificed. Blood and bone marrow were collected, and hematological profiling was undertaken by determining platelet, red blood cell (RBC), white blood cell (WBC), and bone marrow cell counts using a Coulter counter T-890 (Coulter Electronics, U.S.). Heart, liver, kidney, brain, lung, spleen, and thymus were removed and weighed. The organ index and histopathology were investigated for systemic toxicity evaluation: organ index (%) = (organ weight/body weight) × 100.

4.2.9. Histopathologic Evaluation. All tumor and organs from each group were chosen for histopathologic evaluation at tested times. Lungs and tumor were fixed in 10% formaldehyde for 24 h and processed in paraffin. Sections were stained with H&E for examination for histopathologic change.

4.2.10. Data Analysis. All data are presented as the mean ± SD and analyzed using Student's t test or analysis of variance (ANOVA) followed by q test: compared with control, (∗) $p < 0.05$, (∗∗) $p < 0.01$ as significant.

■ AUTHOR INFORMATION

Corresponding Author

*For S.X.: phone, 86-13938637212; e-mail, kfxsq@yahoo.com.cn. For C.W.: phone, 86-13619810550; fax, 86-378-2864665; e-mail, wcjsxq@henu.edu.cn.

Notes

The authors declare no competing financial interest.

■ ABBREVIATIONS USED

N-BDMPrNDI, 2,7-bis[(2-dimethylamino)ethyl]benzo[*lmn*]-[3,8] phenanthroline-1,3,6,8(2*H*,7*H*)-tetraone; MNISpd, 2-{3-[4-(3-aminopropylamino)butylamino]propyl}-1*H*-benz[*de*]-isoquinoline-1,3(2*H*)-dione trihydrochloride; MNIHspd, 2-{4-[4-(4-aminobutylamino)butylamino]butyl}-1*H*-benz[*de*]-isoquinoline-1,3(2*H*)-dione trihydrochloride; Boc, *tert*-butyloxy-carbonyl; MTT, 3-(4,5-dimethylthiazol-2-yl)-2,5-diphenyltetra-zolium bromide; HCS, high content screening; MMP, mitochondrial membrane potential; LMP, lysosomal membrane permeability; PI, propidium iodide; PS, phosphatidylserine; FITC, fluorescein isothiocyanate; ROS, reactive oxygen species; PAO, polyamine oxidase; DCFH-DA, 2′,7′-dichlorodihydro-fluorescein diacetate; MST, median survival time; PBS, phosphate buffered saline; CM-H2DCFDA, 5(and 6)-chlor-omethyl-2′,7′-dichlorodihydrofluorescein diacetate, acetyl ester; RFU, relative fluorescence unit; RBC, red blood cell; WBC, white blood cell; TBAB, tetrabutyl ammonium bromide; TLC, thin-layer chromatography; FCS, fetal calf serum

■ REFERENCES

(1) Giannopoulos, K.; Dmoszynska, A.; Kowal, M.; Wasik-Szczepanek, E.; Bojarska-Junak, A.; Rolinski, J.; Döhner, H.; Stilgenbauer, S.; Bullinger, L. Thalidomide exerts distinct molecular antileukemic effects and combined thalidomide/fludarabine therapy is clinically effective in high-risk chronic lymphocytic leukemia. *Leukemia* 2009, 23 (10), 1771−1778.

(2) Warren, K. E.; Goldman, S; Pollack, I. F.; Fangusaro, J.; Schaiquevich, P.; Stewart, C. F.; Wallace, D.; Blaney, S. M.; Packer, R.; Macdonald, T.; Jakacki, R.; Boyett, J. M.; Kun, L. E. Phase I trial of lenalidomide in pediatric patients with recurrent, refractory, or progressive primary CNS tumors: Pediatric Brain Tumor Consortium study PBTC-018. *J. Clin. Oncol.* 2011, 29 (3), 324−329.

(3) Lv, M.; Xu, H. Overview of naphthalimide analogs as anticancer agents. *Curr. Med. Chem.* 2009, 16 (36), 4797−4813.

(4) Ingrassia, L.; Lefranc, F.; Kiss, R.; Mijatovic, T. Naphthalimides and azonafides as promising anti-cancer agents. *Curr. Med. Chem.* 2009, 16 (10), 1192−1213.

(5) See http://clinicaltrials.gov. Identifiers: NCT01066494, NCT00715637.

(6) Peduto, A.; Pagano, B.; Petronzi, C.; Massa, A.; Esposito, V.; Virgilio, A.; Paduano, F.; Trapasso, F.; Fiorito, F.; Florio, S.; Giancola, C.; Galeone, A.; Filosa, R. Design, synthesis, biophysical and biological studies of trisubstituted naphthalimides as G quadruplex ligands. *Bioorg. Med. Chem.* 2011, 19 (21), 6419−6429.

(7) Liu, Y.; Norton, J. T.; Witschi, M. A.; Xu, Q.; Lou, G.; Wang, C.; Appella, D. H.; Chen, Z.; Huang, S. Methoxyethylamino-numonafide is an efficacious and minimally toxic amonafide derivative in murine models of human cancer. *Neoplasia.* 2011, 13 (5), 453−460.

(8) Van Quaquebeke, E.; Mahieu, T.; Dumont, P.; Dewelle, J.; Ribaucur, F.; Simon, G.; Sauvage, S.; Gaussin, J. F.; Tuti, J.; EI Yazidi, M.; Van Vynckt, F.; Mijatovic, T.; Lefranc, F.; Darro, F.; Kiss, R. 2,2,2-Trichloro-*N*-({2-[2-(dimethylamino)ethyl]-1,3-dioxo-2,3-dihydro-1*H*-benzo[*de*]isoquinolin-5-yl}carbamoyl)acetamide (UNBS3157), a novel nonhematotoxic naphthalimide derivative with potent antitumor activity. *J. Med. Chem.* 2007, 50 (17), 4122−4134.

(9) Chen, Z.; Liang, X.; Zhang, H.; Xie, H.; Liu, J.; Xu, Y.; Zhu, W.; Wang, Y.; Wang, X.; Tan, S.; Kuang, D.; Qian, X. A new class of naphthalimide-based antitumor agents that inhibit topoisomerase II and induce lysosomal membrane permeabilization and apoptosis. *J. Med. Chem.* 2010, 53 (6), 2589−2600.

(10) Liu, Z. R.; Hecker, K. H.; Rill, R. L. Selective DNA binding of (*N*-alkylamine)-substituted naphthalene imides and diimides to G+C-rich DNA. *J. Biomol. Struct. Dyn.* 1996, 14 (3), 331−339.

(11) Tumiatti, V.; Milelli, A.; Minarini, A.; Micco, M.; Gasperi Campani, A.; Roncuzzi, L.; Baiocchi, D.; Marinello, J.; Capranico, G.; Zini, M.; Stefanelli, C.; Melchiorre, C. Design, synthesis, and biological evaluation of substituted naphthalene imides and diimides as anticancer agent. *J. Med. Chem.* 2009, 52 (23), 7873−7877.

(12) Casero, R. A. Jr; Woster, P. M. Recent advances in the development of polyamine analogues as antitumor agents. *J. Med. Chem.* 2009, 52 (15), 4551−4573.

(13) Casero, R. A. Jr.; Woster, P. M. Terminally alkylated polyamine analogues as chemotherapeutic agents. *J. Med. Chem.* 2001, 44 (1), 1−26.

(14) Carta, F.; Temperini, C.; Innocenti, A.; Scozzafava, A.; Kaila, K.; Supuran, C. T. Polyamines inhibit carbonic anhydrases by anchoring to the zinc-coordinated water molecule. *J. Med. Chem.* 2010, 53 (15), 5511−5522.

(15) Weisell, J.; Hyvönen, M. T.; Häkkinen, M. R.; Grigorenko, N. A.; Pietilä, M.; Lampinen, A.; Kochetkov, S. N.; Alhonen, L.; Vepsäläinen, J.; Keinänen, T. A.; Khomutov, A. R. Synthesis and biological characterization of novel charge-deficient spermine ana-logues. *J. Med. Chem.* 2010, 53 (15), 5738−5748.

(16) Tomasi, S.; Renault, J.; Martin, B.; Duhieu, S.; Cerec, V.; Le Roch, M.; Uriac, P.; Delcros, J. G. Targeting the polyamine transport system with benzazepine- and azepine-polyamine conjugates. *J. Med. Chem.* 2010, 53 (21), 7647−7663.

(17) Palmer, A. J.; Wallace, H. M. The polyamine transport system as a target for anticancer drug development. *Amino Acids* 2010, 38 (2), 415−422.

(18) Xie, S.; Wang, J.; Zhang, Y.; Wang, C. Antitumor conjugates with polyamine vectors and their molecular mechanisms. *Expert Opin. Drug Delivery* 2010, 7 (9), 1049−1061.

(19) Kruczynski, A.; Vandenberghe, I.; Pillon, A.; Pesenl, S.; Goetsch, L.; Barret, J. M.; Guminski, Y.; Le Pape, A.; Imbert, T.; Bailly, C.; Guilbaud, N. Preclinical activity of F14512, designed to target tumors expressing anactive polyamine transport system. *Invest. New Drugs* 2011, 29 (1), 9−21.

(20) Barret, J. M.; Kruczynski, A.; Vispé, S.; Annereau, J. P.; Brel, V.; Guminski, Y.; Delcros, J. G.; Lansiaux, A.; Guilbaud, N.; Imbert, T.; Bailly, C. F14512, a potent antitumor agent targeting topoisomerase II vectored into cancer cells via the polyamine transport system. *Cancer Res.* 2008, 68 (23), 9845−9853.

(21) Oliveira, J.; Ralton, L.; Tavares, J.; Codeiro-da-Silva, A.; Bestwick, C. S.; McPherson, A.; Thoo Lin, P. K. The synthesis and the in vitro cytotoxicity studies of bisnaphthalimidopropyl polyamine derivatives against colon cancer cells and parasite *Leishmania infantum*. *Bioorg. Med. Chem.* 2007, 15 (1), 541−545.

(22) Antonini, I.; Volpini, R; Dal Ben, D.; Lambertucci, C.; Cristalli, G. Design, synthesis, and biological evaluation of new mitonafide derivatives as potential antitumor drugs. *Bioorg. Med. Chem.* 2008, 16 (18), 8440−8446.

(23) Tian, Z. Y.; Xie, S. Q.; Du, Y. W.; Ma, Y. F.; Zhao, J; Gao, W. Y.; Wang, C. J. Synthesis, cytotoxicity and apoptosis of naphthalimide polyamine conjugates as antitumor agents. *Eur. J. Med. Chem.* 2009, 44 (1), 393−399.

(24) Tian, Z. Y.; Xie, S. Q.; Mei, Z. H.; Zhao, J.; Gao, W. Y.; Wang, C. J. Conjugation of substituted naphthalimides to polyamines as cytotoxic agents targeting the Akt/mTOR signal pathway. *Org. Biomol. Chem.* 2009, 7 (22), 4651−4660.

(25) Yang, L.; Zhao, J.; Zhu, Y.; Tian, Z.; Wang, C. Reactive oxygen species (ROS) accumulation induced by mononaphthalimide-spermidine leads to intrinsic and AIF-mediated apoptosis in HeLa cells. *Oncol. Rep.* 2011, 25 (4), 1099−1107.

(26) Sakurai, H.; Tsukuda, T.; Hirao, T. Pd/C as a reusable catalyst for the coupling reaction of halophenols and arylboronic acids in aqueous media. *J. Org. Chem.* 2002, 67 (8), 2721−2722.

(27) Xie, L.; Cui, J.; Qian, X.; Xu, Y.; Liu, J.; Xu, R. 5-Non-amino aromatic substituted naphthalimides as potential antitumor agents: synthesis via Suzuki reaction, antiproliferative activity, and DNA-binding behavior. *Bioorg. Med. Chem.* **2011**, *19* (2), 961−967.

(28) Tumiatti, V.; Milelli, A.; Minarini, A.; Rosini, M.; Bolognesi, M. L.; Micco, M.; Andrisano, V.; Bartolini, M.; Mancini, F.; Recanatini, M.; Cavalli, A.; Melchiorre, C. Structure−activity relationships of acetylcholinesterase noncovalent inhibitors based on a polyamine backbone. 4. Further investigation on the inner spacer. *J. Med. Chem.* **2008**, *51* (22), 7308−7312.

(29) O'Brien, P. J.; Irwin, W.; Diaz, D.; Howard-Cofield, E.; Krejsa, C. M.; Slaughter, M. R.; Gao, B.; Kaludercic, N.; Angeline, A.; Bernardi, P.; Brain, P.; Hougham, C. High concordance of drug-induced human hepatotoxicity with invitro cytotoxicity measured in a novel cell-based modelusing high content screening. *Arch. Toxicol.* **2006**, *80* (9), 580−604.

(30) Elmore, S. Apoptosis: a review of programmed cell death. *Toxicol. Pathol.* **2007**, *35* (4), 495−516.

(31) Wang, J.; Wu, A. B.; Xu, Y. F.; Liu, J. W.; Qian, X. H. M2-A induces apoptosis and G2-M arrest via inhibiting PI3 K/Akt pathway in HL60 cells. *Cancer Lett.* **2009**, *283* (2), 193−202.

(32) Sohaebuddin, S. K.; Thevenot, P. T.; Baker, D.; Eaton, J. W.; Tang, L. Nanomaterial cytotoxicity is composition, size,and cell type dependent. *Part. Fibre Toxicol.* **2010**, *7* (22), 2−17.

(33) Lin, B.; Chen, Z.; Xu, Y.; Zhang, H.; Liu, J.; Qian, X. 7-b, a novel amonafide analogue, cause growth inhibition and apoptosis in Raji cells via a ROS-mediated mitochondrial pathway. *Leuk. Res.* **2011**, *35* (5), 646−656.

(34) Mijatovic, T.; Mahieu, T.; Bruyère, C.; De Nève, N.; Dewelle, J.; Simon, G.; Dehoux, M. J.; van der Aar, E.; Haibe-Kains, B.; Bontempi, G.; Decaestecker, C.; Van Quaquebeke, E.; Darro, F.; Kiss, R. UNBS5162, a novel naphthalimide that decreases CXCL chemokine expression in experimental prostate cancers. *Neoplasia* **2008**, *10* (6), 573−586.

(35) Zhu, H.; Miao, Z. H.; Huang, M.; Feng, J. M.; Zhang, Z. X.; Lu, J. J.; Cai, Y. J.; Tong, L. J.; Xu, Y. F.; Qian, X. H.; Ding, J. Naphthalimides induce G2 arrest through the ATM-activated Chk2-executed pathway in HCT116 cells. *Neoplasia* **2009**, *11* (11), 1226−1234.